Received: 27 August 2018 | Revised: 15 January 2019 | Accepted: 15 January 2019

DOI: 10.1002/jrs.5567

RESEARCH ARTICLE

WILEY Journal of RAMAN SPECTROSCOPY

Amyloid formation kinetics of hen egg white lysozyme under heat and acidic conditions revealed by Raman spectroscopy

Lei Xing | Wei Fan | Ning Chen | Mengna Li | Xiaoguo Zhou | Shilin Liu

Hefei National Laboratory for Physical Sciences at the Microscale, iChEM (Collaborative Innovation Center of Chemistry for Energy Materials), Department of Chemical Physics, University of Science and Technology of China, Hefei, China

Correspondence
Xiaoguo Zhou and Shilin Liu, Hefei National Laboratory for Physical Sciences at the Microscale, iChEM (Collaborative Innovation Center of Chemistry for Energy Materials), Department of Chemical Physics, University of Science and Technology of China, Hefei 230026, China.
Email: xzhou@ustc.edu.cn; slliu@ustc.edu.cn

Funding information
National Key Basic Research Foundation of China, Grant/Award Number: 2013CB834602; National Natural Science Foundation of China, Grant/Award Numbers: 21573208, 21573210 and 21873089

Abstract

Amyloid fibrillation of proteins is a hallmark of neurodegenerative disease, accompanied by the formation of the organized cross-β cores. This conformational transformation is considered to be related to the toxicity underlying the pathogenic mechanism. However, the exact conformational transformation kinetics of amyloid fibrillation are not fully understood. Herein, Raman spectroscopy was used to detect the transformation in the molecular structure of hen egg white lysozyme during amyloid formation under heat and acidic conditions (pH 2.0 and 65°C). The overall kinetics of the hen egg white lysozyme conformational change were investigated by analyzing five characteristic spectral fingerprints. The two N—C_α—C stretching bands at 899 and 935 cm^{-1} and the amide I band (at 1,640–1,680 cm^{-1}) correlated to the lysozyme skeleton structure, whereas the band of the Phe amino acid group in side chains at 1,003 cm^{-1} and the two Trp residue bands at 760 and 1,340–1,360 cm^{-1} were associated with the tertiary structure. Based on these results, a four-stage step-by-step transformation mechanism is first proposed to describe the exact kinetics of lysozyme amyloid fibrillation under heat and acidic conditions. This provides necessary information for physiologists to artificially control the amyloid formation of neurodegenerative disease patients.

KEYWORDS

Alzheimer's disease, amyloid fibrils, kinetics, lysozyme, Raman spectroscopy

1 | INTRODUCTION

Amyloid formation is a conformational change of native proteins that is often associated with protein degradation, degeneration, and cell toxicity, leading to neurodegenerative diseases.[1–3] Under environmental shifts, such as variations in pH and temperature, amyloid formation of a protein begins with partial unfolding of the native state, followed by a series of conformational changes to form the soluble oligomer.[2,4,5] Along with decomposition and aggregation of the oligomers, the long protofibrils gradually grow out to form unbranched structures with a diameter of 6–12 nm, in which the ordered β-sheet secondary structures are perpendicular to the fiber axis.[2,6,7]

The amyloid fibrils of many proteins have been reported, demonstrating common morphological characteristics, such as insulin, bovine serum albumin, and hen egg white lysozyme (HEWL).[8–14] As a simple protein, HEWL has 129 amino acid residues, a molecular weight of approximately 14.3 kDa, and a predominantly α-helical conformation. HEWL shows 40% amino acid sequence identity with human lysozyme, and its amyloid

fibrillation is very similar to that of amyloid-β proteins associated with Alzheimer's disease.[8,15–19] Under specific experimental conditions, lysozyme amyloid fibrils can be formed, accompanying by conformation changes of the residues 57 to 107.[20] Thus, HEWL has been widely used as a model protein to investigate the mechanisms of amyloid formation. However, HEWL is more stable than amyloid-β 1–40 proteins under physiological conditions, and hence, harsher conditions are required for amyloid fibrillation to effectively denature and form the fibrils within an acceptable experimental timescale.

Many studies have successfully observed the morphological changes of lysozyme during amyloid fibrillation under heat and acidic conditions.[21–25] On the basis of measurements of the hydrodynamic radius and total scattering intensity, Jain and Udgaonkar[26] found a time delay between the formation of worm-like protofibrils and their lateral association, providing conclusive evidence of a multistep mechanism of amyloid fibrillation. Dynamic light scattering and atomic force microscopy (AFM) experiments further suggested that the amyloid fibril assembly of lysozyme followed a strict hierarchical aggregation routine, in a so-called on-pathway from the amyloid monomers, oligomers, protofibrils, and more complex structures.[27] In addition, the very distinct amorphous aggregates of HEWL were found to be formed following disulfide-reducing treatment, implying an alternate pathway for protein aggregation.[28,29]

In addition to these morphological measurements, many spectroscopic approaches have been employed to study amyloid formation. Owing to its high sensitivity, Fourier transform-infrared (FT-IR) spectroscopy has been extensively applied to detect the secondary structure of proteins. For example, Li et al.[30] combined FT-IR spectral analyses and static light scattering measurement to verify that the secondary structure transformation of lysozyme occurred before fibril growth. Ma and colleagues[7,8] also found that at elevated temperature, fibrils with a parallel β-sheet configuration formed via transforming the oligomers of an antiparallel β-sheet structure under room temperature.

However, the H–D exchange effect is an inevitable consequence of obtaining IR spectra in deuterated aqueous solution. More importantly, many aromatic amino acid side chains have an IR intensity that is too weak to be detected in aqueous solutions, although the spectral information of these residues is very useful to characterize the protein tertiary structure. Fortunately, the vibrations of the side chains and skeletons have visible Raman intensities in aqueous proteins, especially the aromatic amino acid residues such as Phe, Tyr, and Trp. Moreover, their Raman shifts, intensities, and bandwidths are very sensitive to local environmental conditions. Therefore, Raman spectroscopy has advantages for identification of protein conformation and has been successfully utilized to detect the structure changes occurring at all stages of the formation of insoluble and noncrystalline protein aggregates.[12,31–38] Through analyzing the amide I, II, and III bands in deep ultraviolet Raman spectra, a disordered secondary structure (the so-called statistical coil) was verified to be initially formed,[36] followed by assembly to β-sheet-rich oligomers. Consequently, the oligomers aggregated in multiple assembly states forming a nucleus, so that a large number of nuclei ultimately rapidly propagated into filaments and fibrils.[39] Besides these secondary structure changes, the intensity decrease of both the Phe and Tyr bands indicated that the microenvironments of the side groups changed, and the Phe and Tyr groups were exposed to the aqueous environment.[40,41] In addition, a Tip-enhanced Raman spectroscopic investigation suggested that the aromatic amino acid residues were almost equally distributed over the β-sheet and α-helix/unordered regions on the protein surface.[32] An excellent review was recently published that summarizes the progress in Raman spectral studies on amyloid fibrils formation.[24]

Although the lysozyme structures before and after amyloid fibrillation are well known,[7,8,12,24,32,36,42–45] the exact transformation kinetics of amyloid fibrillation remain incompletely understood. To resolve these questions, in the present study, we have applied a combined spectroscopic approach to investigate the changes in the molecular structure transformation of HEWL over incubation time during amyloid formation under heat and acidic conditions (pH 2.0 and 65°C). The morphology of lysozyme can be directly observed by AFM, whereas the thioflavin T (ThT) fluorescence measurement provides information on the population change of the cross β-sheets.[46–48] The secondary and tertiary structure changes of the aqueous lysozyme during amyloid formation were then detected in situ by Raman spectroscopy. Through analyzing the Raman marker changes of the skeleton and side chain vibrations over incubation time, a multistep kinetic mechanism is proposed to fully describe the amyloid fibrillation of lysozyme under heat and acidic conditions. This will shed lights on artificial administration of amyloid formation in the future.

2 | EXPERIMENTAL

2.1 | Solution preparation

HEWL was purchased from Sangon Biotech (Shanghai) Co. Ltd and used without further purification. Lysozyme

amyloid fibrillation was performed as described previously.[36,45,49] In brief, the concentration of lysozyme was 20 mg/ml in the aqueous solution, and the pH was set to 2.0 with the addition of hydrochloric acid. The solutions in sealed glass vials were incubated in a thermoshaker at 65°C without agitation. At various incubation times, an aliquot of the fibril-forming solution was taken out of the vial, and the gelatinous phase was mainly separated by centrifugation at 12,000 *g* for 20 min. The aliquoted supernatant was then directly used in the Raman spectroscopy, ThT fluorescence assay, and AFM experiments. Because the supernatant separated by centrifugation contains only a small amount of protein gels,[43] a certain amount of the mature fibrils was still suspended in the supernatant. Thus, the spectral characteristics of the mature fibrils could be observed in the Raman spectra of the supernatant.

2.2 | Raman spectra

The Raman spectrometer used in this study has been described in detail previously.[50–54] In brief, a CW laser (Coherent, 532 nm) with a power of 4 W was employed as the excitation light. The Raman scattering light was dispersed by a triple-monochromator system (Acton Research, TriplePro) and recorded in the region of 300–1,850 cm^{-1} by a liquid nitrogen-cooled CCD detector (Princeton Instruments, Spec-10:100B) at a spectral resolution of ~1 cm^{-1}. The Raman shift was carefully calibrated using the standard spectral line of a mercury lamp. The sample solution was kept in a 10 × 10-mm quartz cuvette. The acquisition time was ~55 s for each measurement, and then the Raman spectrum was accumulated and averaged by 20 acquisitions and was subtracted by the spectrum of the acidic solution measured under identical conditions.

2.3 | AFM images

All AFM images were acquired on air-dried samples using a Veeco DI-MultiMode V scanning probe microscope in tapping mode. A 5 × 5-μm scanner was used in the present experiments. The protein solution was diluted 100 times with Milli-Q water and then dropped onto the freshly cleaved mica. Fifteen minutes later, the protein solution was rinsed off with deionized water three times. The mica surface was dried at room temperature, and the sample was stored in a desiccator. The AFM images were represented using an open-access software from Nanoscope Inc.

2.4 | ThT fluorescence assay

The steady-state fluorescence emission was measured using a fluorescence spectrophotometer (F-4600, Shimadzu) within a wavelength range of 400–800 nm. An excitation wavelength at 420 nm was used, and emission at 480 nm was chosen to represent the fluorescence intensity. The concentration of the ThT solution was 1×10^{-5} mol/L. During amyloid fibrillation, 40 μl of the aliquoted supernatant was taken out of the vial at various incubation times and added to 960 μl of the ThT solution. The assay was performed ex situ for the mixed solution immediately. Five acquisitions were averaged to obtain the final intensity at each incubation time. All measurements were performed under ambient conditions.

3 | RESULTS AND DISCUSSION

3.1 | AFM images during amyloid fibrillation of lysozyme

Representative AFM images of lysozyme at various incubation times are shown in Figure 1. Under the heat and acidic conditions, no fibril formed at the very early incubation stage of the aqueous lysozyme solution, because lysozyme in the native state was too small to be observed. Several hours later, heterogeneously sized spheroidal oligomers appeared, which grew larger with aggregation (Figure 1b). With the increase of incubation time, the spheroidal oligomers gradually self-assembled to protofibrils with an average diameter of 8 nm (Figure 1 c). After incubation for 4 days, the mature lysozyme fibrils were clearly observed (Figure 1d), which were approximately a few microns in length and looked slightly stiffer than the protofibrils.

3.2 | ThT fluorescence of lysozyme in the native state and the mature fibrils

The fluorescence of ThT dye can be enhanced with formation of amyloid fibrils, because the surfaces of cross β-sheet structures in proteins form ThT-binding sites.[46–48] Thus, an increase in the ThT fluorescence intensity is a good indicator to verify and quantify the formation of cross β-sheet-rich structures during amyloid fibrillation. In the present experiment, the dye was added to the aqueous lysozyme solution and incubated under the same thermal and acidic conditions. Figure 2 shows the fluorescence spectra of lysozyme in the native state and the mature fibrils. The fluorescence intensity was remarkably enhanced after amyloid fibrillation by approximately 13-fold, indicating that a large

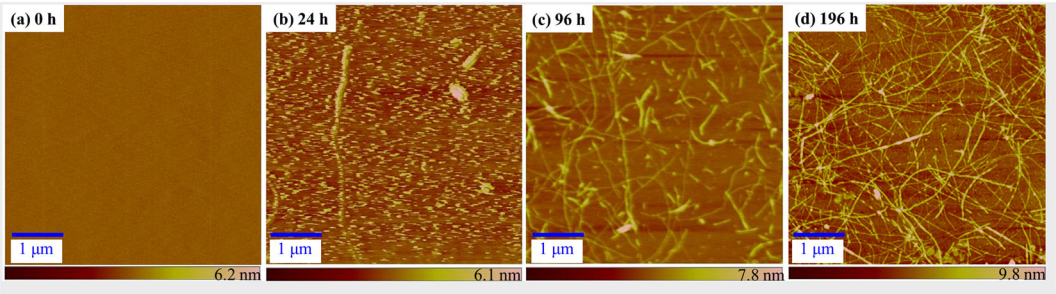

FIGURE 1 Atomic force microscopy height images of aqueous lysozyme incubated at 65°C and pH 2.0 for 0 hr (a), 24 hr (b), 96 hr (c), and 196 hr (d), using a 5 × 5-μm scanner [Colour figure can be viewed at wileyonlinelibrary.com]

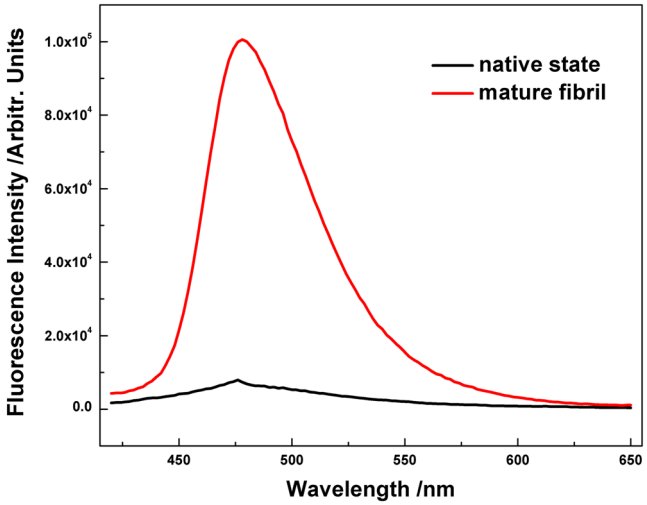

FIGURE 2 Thioflavin T fluorescence spectra of lysozyme in the native state (black line) and the mature fibrils (red line) [Colour figure can be viewed at wileyonlinelibrary.com]

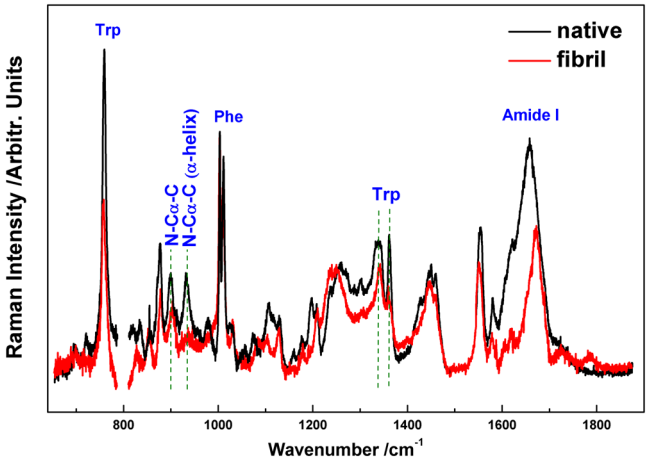

FIGURE 3 Overall Raman spectra of lysozyme in the native state (black) and the mature fibrils (red) in the range of 650–1,875 cm^{-1}; both intensities were normalized by the Phe band at 1,003 cm^{-1} [Colour figure can be viewed at wileyonlinelibrary.com]

amount of cross β-sheet-rich structures were formed in the mature fibrils. These results from AFM imaging and ThT fluorescence measurements are consistent with previous investigations.[7,49]

3.3 | Raman spectra of lysozyme in the native state and the mature fibrils

Under the heat and acidic conditions, both the secondary and tertiary structures of the aqueous lysozyme gradually changed. The overall Raman spectra in the range of 650–1,875 cm^{-1} of lysozyme in the native state and the mature fibrils were respectively recorded (Figure 3). All of the band intensities of the mature fibrils were much weaker than those detected in the native state, which was attributed to the decreased concentration of protein in the supernatant during amyloid fibrillation. Thus, the band intensities shown in Figure 3 were normalized to the Phe amino acid band at 1,003 cm^{-1} for effective comparison. Moreover, Raman spectra of the supernatant after being incubated for 220 h and the gelation after lyophilization were recorded by the confocal micro-Raman spectrometer and shown as Figure S1 of the supporting information. The almost identical spectra were observed.

Because some vibrational bands of acidic water existed in the region, the Raman spectra of lysozyme in the supernatant were subtracted by the acid–water spectra measured under the same conditions. Because it was not feasible to perform qualitative and quantitative analyses for all of the vibrational bands shown in Figure 3, only a few well-known vibrational bands were selected for quantitative analysis of the denaturation of lysozyme under the heat and acidic conditions. These bands were classified into those of the skeletons and side groups of lysozyme. The N—C_α—C stretching and amide I bands were chosen to monitor the conformational transformations of the skeleton, whereas the vibrational bands contributed by the Trp and Phe amino acid residues were utilized to indicate the local environmental changes of the side chains. The functional groups, Raman shifts, and vibrational assignments of these Raman bands are summarized in Table 1, as well

TABLE 1 Assignments of the specific Raman bands of lysozyme in the native state

Molecular groups	Raman shift/cm^{-1}[a]	Assignment	Raman marker
Trp	759 (759)	Coupled vibrations of in-phase breathings of benzene and pyrrole	FWHM[55,56]
N—C_α—C	899 (905) 932 (935)	N—C_α—C stretching Stretching of N—C_α—C in the α-helical structure	FWHM/wave number shift[55,57–60] Intensity[55,57–60]
Phe	1,003 (1,003)	Ring breathing of benzene in the Phe amino residue	FWHM[58,59]
Trp	1,340/1,360 (1,340/1,360)	Fermi resonances between the fundamental in-plane N1=C8 stretching and combination bands of ring out-of-plane deformations	Intensity ratio $I_{1,340}/I_{1,360}$[57,58,61]
Amide	1,658 (1,671)	"Amide I" as the coupling mode of the C=O and C—N stretching vibration and a small amount of N—H in-plane bending vibration	Wave number shift[59,62]

Note. FWHM: full width at half maximum.

[a]The values in parentheses are the Raman shifts of the mature fibrils.

as the corresponding Raman markers during amyloid fibrillation. Figure 4 shows the partially magnified Raman spectra of these specific bands in the regions of 730–785, 885–1,022, 1,310–1,370, and 1,580–1,720 cm^{-1}.

3.3.1 | Skeleton

The bands at both 899 and 935 cm^{-1} are well known to be attributed to the N—C_α—C stretching vibrations of the lysozyme skeletons, and the latter band is mainly associated with α-helical secondary structures.[55,57–60] Both bands are very sensitive to the conformation of N—C_α—C segments. For the band at 899 cm^{-1}, the full width at half maximum (FWHM) was broadened, and the peak position was blue-shifted when the conformations of the N—C_α—C skeletons became variegated to induce various rotational isomers with slightly different vibrational frequencies after denaturation.[55] The intensity of the N—C_α—C stretching at 935 cm^{-1} is correlated to the population of α-helical structures.[57] As shown in Figure 4b, the peak position of the N—C_α—C stretching

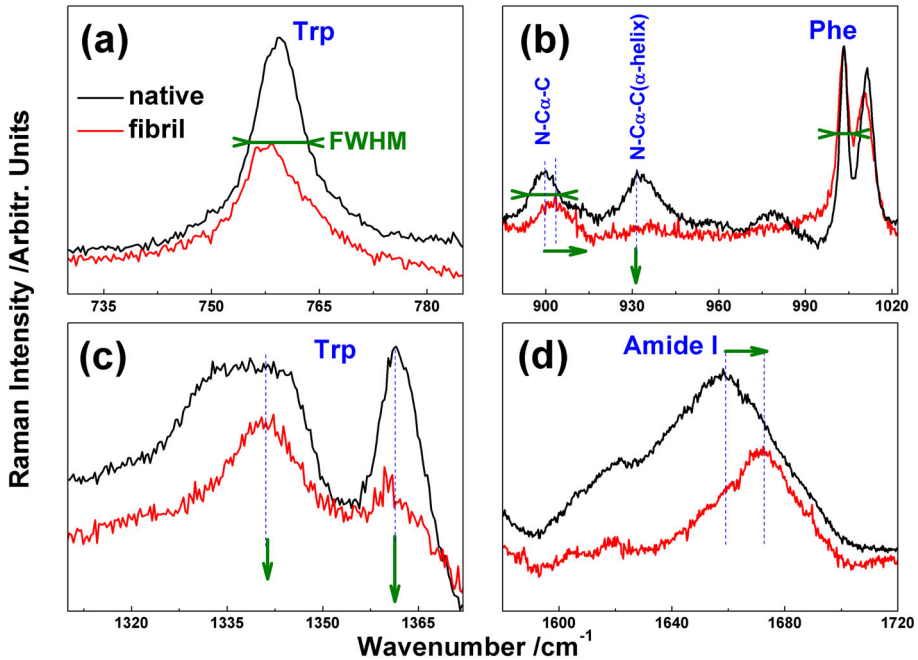

FIGURE 4 Partially magnified Raman spectra of lysozyme in the native state (black) and the mature fibrils (red) in the range of (a) 730–785 cm^{-1}, (b) 885–1,022 cm^{-1}, (c) 1,310–1,370 cm^{-1}, and (d) 1,580–1,720 cm^{-1}. FWHM: full width at half maximum [Colour figure can be viewed at wileyonlinelibrary.com]

band was blue-shifted from 899 cm^{-1} in the native state to 904 cm^{-1} in the mature fibrils, and its FWHM increased from 11 to 18 cm^{-1}, implying the conformational transformation of the N—C_α—C skeleton. Because the N—C_α—C stretching intensity at 935 cm^{-1} is proportional to the population of α-helical secondary structures, the markedly reduced intensity from the native state to the fibrils indicated the dramatic loss of α-helical structures during amyloid formation, which is consistent with previous conclusions.[43,45,63]

The peak centered at 1,658 cm^{-1} is referred to as the "amide I" band, which consists of the coupling mode of the C=O and C—N stretching vibrations and a small amount of the N—H in-plane bending vibration.[59,62] Thus, the amide I band is another important spectral probe of the protein skeleton structure. As indicated in previous studies,[24,34,40] the strong amide I band reflects the contributions of various secondary structures and is sensitive to conformational changes because the corresponding Raman shift depends on the strength of the hydrogen bonding interaction (C=O···H) involving the amide groups and the dipole–dipole interaction between the carboxyl groups. Thus, the different frequencies are correlated with specific secondary structures. However, the corresponding wave number regions remain controversial.

In traditional Raman spectral analysis, the α-helical structure is usually located in the 1,640–1,654 cm^{-1} range; the organized β-sheets are in the range of 1,665–1,680 cm^{-1}, and the disordered structures, including the β-turns, loose β-strands, and polyproline structures, appear in the 1,654–1,665 cm^{-1} region.[35,42,44,48,49] Recent FT-IR investigations suggested slightly different assignments[7,8]; however, owing to the H–D exchange effect in the IR spectra of the deuterated aqueous solution as well as the different cross sections in Raman and IR spectra, the classic Raman vibrational assignments were utilized in the present analyses of the transformation of the α-helix, disordered structures, and organized β-sheets. In addition, the amide I position in the Raman spectra could not be used to determine the β-sheet conformations due to the indistinguishable contributions of the parallel and antiparallel β-sheets.[64,65]

When organized β-sheets are dominantly formed, the amide I position is expected to be blue-shifted. Indeed, as shown in Figure 4d, a blue shift of 12 cm^{-1} was detected for the amide I band from the native state to the fibrils, and a narrower FWHM was also observed. Collectively, the spectral changes indicated that the α-helical secondary structures of lysozyme were transformed to other conformations such as β-sheets or statistical coils during amyloid fibrillation. In the mature fibrils, the dominant secondary structures were the organized β-sheets. The kinetic details are discussed in the following section.

3.3.2 | Side chains

Besides the vibrational bands described above, a few vibrational bands of aromatic amino acid residues located in the side chains of lysozyme were also detected in the Raman spectra shown in Figure 4. The sharp peak at 759 cm^{-1} is assigned to the coupled vibrations of the in-phase symmetric ring breathings of benzene and pyrrole of the Trp residue.[55,56] Thus, it is delocalized over the indole ring, and its intensity is very sensitive to the distortion of the indole ring affected by the local environment. The double peaks at 1,340 and 1,360 cm^{-1} are assigned as the Fermi resonances between the fundamental in-plane N_1=C_8 stretching and the combination bands of ring out-of-plane deformations. The relative intensity ratio of the doublet, $I_{1,340}/I_{1,360}$, has been suggested to be a good indicator of the local environment of the Trp indole ring.[57,58,61] When $I_{1,340}/I_{1,360}$ is less than 1.0, the indole ring of Trp is in a hydrophobic environment, and otherwise, it is exposed to the aqueous medium or is in contact with the aliphatic side chains.[58,66,67] The band at 1,003 cm^{-1} is assigned as the ring breathing of benzene in the Phe amino acid residue.[58,59] Similar to the Trp band at 759 cm^{-1}, the FWHM at 1,003 cm^{-1} becomes wider when the protein tertiary structure is loosened and the Phe residues are exposed to the outside. During amyloid fibrillation, the initial rigid configuration transforms into various rotational isomers with different vibrational frequencies, consequently resulting in the broadening and weakening of their Raman bands. Therefore, the changes of these Raman spectral markers can reflect transformation of the tertiary structure.

As shown in Figure 4a, the FWHM of the Trp band at 759 cm^{-1} was increased from 7 cm^{-1} in the native state to 12 cm^{-1} in the mature fibrils, and its intensity was dramatically decreased at the same time. These spectral changes demonstrated that the coupling between the in-phase ring breathing vibrations of benzene and pyrrole was weakened in the fibrils owing to distortion of the indole ring, and the conformations of the Trp groups became more variegated. Moreover, the intensity ratio, $I_{1,340}/I_{1,360}$, markedly increased to a value larger than 1.0 in the mature fibrils. This indicated that the Trp residues in the mature fibrils were exposed to a hydrophilic environment, which was consistent with the deductive conclusions of the Trp band. In addition, the FWHM of the Phe band at 1,003 cm^{-1} increased from 4 cm^{-1} in the native state to 7 cm^{-1} in the fibrils. Therefore, during amyloid fibrillation, the microenvironments of the Trp and Phe amino acid side groups were changed, which were closely associated with transformation of the lysozyme tertiary structure.

3.4 | Kinetics of Raman markers during amyloid fibrillation

As mentioned above, the exact kinetics of lysozyme during amyloid fibrillation are not fully known despite extensive investigations on the changes of the secondary and tertiary structures before and after amyloid fibrillation. Using the Raman markers, we evaluated the time-dependent structure changes of lysozyme during amyloid fibrillation under heat and acidic conditions. Figures 5 and 6 show the time-dependent curves of the markers for the side chains and skeleton, respectively, over incubation time from 0 to 210 hr. The corresponding spectra were summarized in the supporting information.

The curves of the Trp and Phe residues displayed single exponential growth functions. After incubation at pH 2.0 and 65°C, the tertiary structure of lysozyme in the aqueous solution was immediately unfolded, and the Trp and Phe residues of the side chains were consequently exposed to a hydrophilic environment as indicated by the Raman markers of Trp bands (FWHM at 759 cm^{-1} and the intensity ratio, $I_{1,340}/I_{1,360}$) and the Phe band (FWHM at 1,003 cm^{-1}). After incubation for about 40 hr, the growth rates of the markers reduced, and all markers finally increased to saturation at about 90 hr of incubation, implying that all of the Trp and Phe residues were nearly completely exposed to the hydrophilic environment on the protein surface, and the related tertiary structure was thoroughly destroyed.

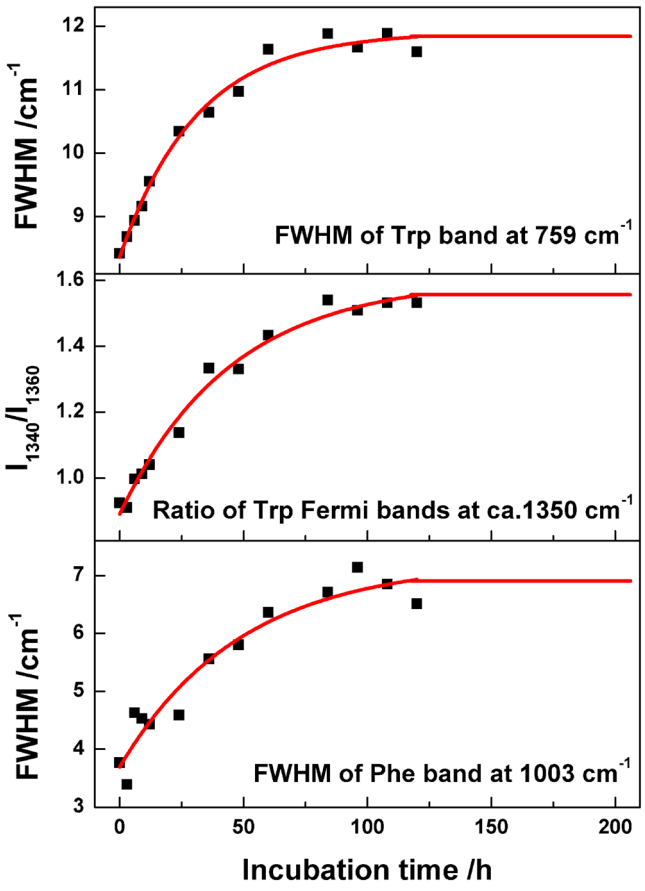

FIGURE 5 Time-dependent curves of the Raman markers for the side chains. The black points are the measured values at various incubation times, and the red traces are the fitted curves. FWHM: full width at half maximum [Colour figure can be viewed at wileyonlinelibrary.com]

In contrast to the monotonous changes of the Raman markers for the tertiary structure, all of the time-dependent curves of the skeleton markers displayed a sigmoid functional relationship over incubation time (Figure 6). In general, a sigmoid functional relationship indicates that protein aggregation typically undergoes a lag phase, followed by a rapid growth phase and an equilibrium phase. In a two-state mechanism of fibrillation,[2,68] the soluble prefibrillar oligomers aggregate to form a nucleus during the lag phase, and then the nuclear template protein assembles to fibrils.

Notably, the time-dependent curves of the N—C_α—C stretching and the amide I bands exhibited different kinetic behaviors, although they are both located on the skeleton. Thus, the structure transformations in the lag, growth, and equilibrium phases are completely different, which is in agreement with our recent proposal of a multistate mechanism.[69] Both indicators related to N—C_α—C stretching showed almost identical time-dependent behaviors (Figure 6). The duration of the lag phase was only a few hours, and the growth phase lasted to ~37 hr when the tertiary structure related to the Trp and Phe residues was almost fully unfolded. By contrast, the lag duration of the amide I position curve was delayed to ~34 hr, and the growth phase ended at ~84 hr.

Based on the interpretations and kinetics of the skeleton markers, it appears that the α-helical secondary structures of lysozyme are dramatically destroyed prior to the formation of organized β-sheets (Figure 6). Overall, this finding is in agreement with the previous hypothesis that the α-helix prefers to first transform into a statistical coil rather than to organized β-sheets.[36] Oligomerization and fibrillation are the main competing channels during amyloid fibrillation. Accordingly, under a heat and acidic condition, the highly amyloidogenic peptide fragments of 49–101 and 53–101 as well as the nicked HEWL produced from the hydrolysis of HEWL at the Asp residue sites 48 and 101 are the amyloidogenic materials responsible for both the oligomerization and fibrillation.[20]

The spectral profile in the amide I region showed a complicated change during amyloid fibrillation (Figure 7). To exhibit this change in detail, the intensities of the spectrum were normalized by that of the Phe band at 1,003 cm^{-1} measured at the same incubation time and under the same experimental conditions. In contrast to

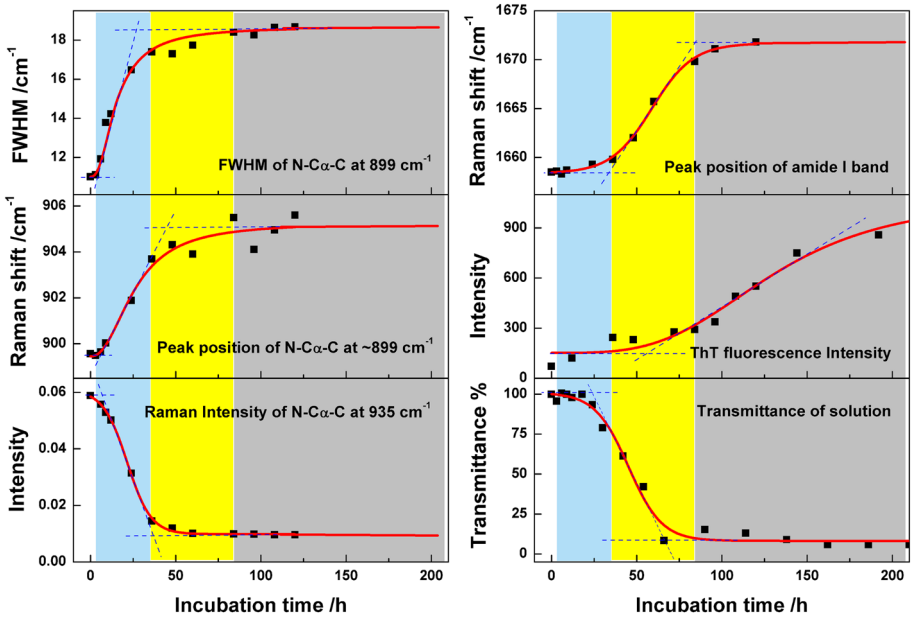

FIGURE 6 Time-dependent curves of Raman markers for the skeletons of lysozyme, as well as the change curve of the thioflavin T (ThT) fluorescence intensity and transmittance of the solution during amyloid fibrillation. The black squares are the experimental data, and the red traces are the fitted curves. The blue shaded region represents the period of the α-helix uncoiling to statistical coils with disordered structure, the yellow one notes the time interval of the formation of organized β-sheets during decomposition of the oligomers into amyloidogenic fragment materials, and the gray region is the period of the dominant formation of cross β-sheet structures with elongation of unbranched protofibrils. FWHM: full width at half maximum [Colour figure can be viewed at wileyonlinelibrary.com]

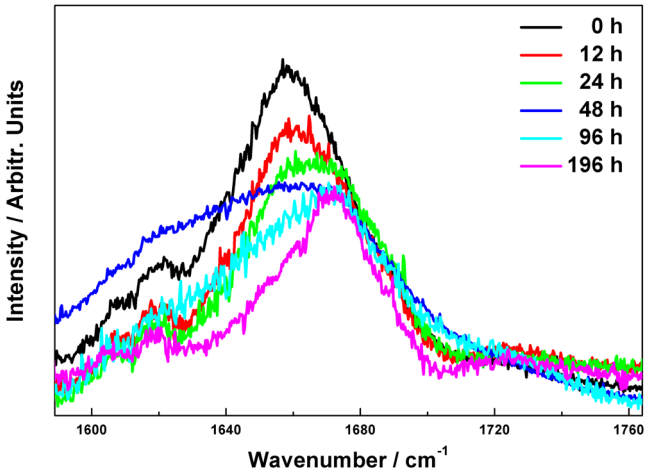

FIGURE 7 Time-dependent Raman spectra of the amide I region; the intensities were normalized by the Phe band at 1,003 cm^{-1} [Colour figure can be viewed at wileyonlinelibrary.com]

the monotonous change of the amide I peak position, the whole FWHM showed an abnormal change relationship with incubation time. The width very slowly increased at the initial stage (for several hours) corresponding to the gradual formation of disordered structures. These disordered structures then aggregate to the cores and oligomers. After incubation for 24 hr, the intensities at 1,652 and 1,674 cm^{-1} were almost equal, associated with the populations of the α-helical and disordered structures (and/or β-sheets), respectively. As a result, the peak position hardly changed although the profile became flat. Subsequently, the band wide dramatically increased, because the intensity of the low wave number side in the region of 1,580–1,640 cm^{-1} significantly enhanced. However, the low wave number tail is attributed to the combination band of the Phe, Tyr, and Trp groups on the side chains[55,56,70] and thus does not correlate to the secondary structures. With increased incubation time, the related intensity ratio at 1,652 and 1,674 cm^{-1} remained reduced, and the width certainly decreased. The mature fibrils with the cross β-sheet-rich conformation finally formed, as the band dominated in the 1,665- to 1,685-cm^{-1} region. All of these spectral changes are consistent with the hypothesis of the conformational transformations of lysozyme from the α-helix to the statistical coil with a disordered structure, finally forming cross β-sheets.

To quantitatively compare these kinetics, Equation (1) of the sigmoid function was used to fit the time-dependence curves in Figures 5 and 6[71–73]:

$$\mathrm{I(t)} = \mathrm{I}_i + \frac{I_f - I_i}{1 + \exp\left[-\dfrac{t - T_m}{\Delta T}\right]}, \quad (1)$$

where I_i and I_f are the spectral parameters (e.g., FWHM, Raman shift, or intensity) of the initial and final states, respectively, T_m is the transition midpoint time, and $2 \times \Delta T$ corresponds to the transition interval. Table 2

TABLE 2 The lag duration (T_0), transition midpoint time (T_m), equilibrium duration (T_e), and a half interval (ΔT) of various skeleton conformation markers during the amyloid fibrillation of lysozyme under heat and acidic conditions

Raman marker	T_0/hr	T_m/hr	T_e/hr	ΔT/hr
FWHM of the N—C_α—C stretching at 899 cm^{-1}	4	15	28	7
Raman shift of the N—C_α—C stretching at 899 cm^{-1}	6	26	44	12
Intensity of the N—C_α—C stretching at 935 cm^{-1}	7	22	37	7
Raman shift of the amide I band at 1,658 cm^{-1}	34	59	84	12
ThT fluorescence intensity	55	119	—	31
Transmittance of the solution	24	45	66	10

Note. FWHM: full width at half maximum; ThT: thioflavin T.

summarizes the derived T_m values of the Raman markers. Here, we define two new parameters, T_0 and T_e, to represent the durations of the lag and equilibrium phases in a two-state mechanism of fibrillation for comparison of the different kinetics in Figure 6. In a typical sigmoid functional curve, T_0 and T_e are approximatively determined as the cross points between the fitted lines of the lag and the growth and equilibrium phases, as shown in Figure 6.

In addition, the kinetic curve of the ThT fluorescence intensity and the transmittance of the lysozyme solution during amyloid formation are plotted in Figure 6. The ThT fluorescence intensity only slightly changed during the initial lag stage and then slowly increased. Obvious enhancement at a relatively quick rate was observed after approximately 90 hr and then tended to saturate. This indicated that the β-sheet-rich structures started to be formed from the statistical coils and quickly assembled during the transformation from the protofibrils to mature fibrils. A similar trend was also observed for the transmittance of the solution. Once the oligomers formed, the transmittance began to decrease. After incubation for approximately 90 hr, the transmittance of the solution became close to its minimal value.

3.5 | Four-stage mechanism of amyloid fibrillation under heat and acidic conditions

Based on the kinetics of the Raman markers in Figures 5 and 6, a four-stage transformation mechanism is tentatively proposed for the amyloid formation of the lysozyme aqueous solution under incubation at pH 2.0 and 65°C, which is summarized in Scheme 1.

At the initial incubation stage (0–10 hr), lysozyme in the aqueous solution immediately starts to unfold from the native state under the action of the heat and acid. Its tertiary structure is partially destroyed, and the Trp and Phe residues of the side chains are exposed to the hydrophilic environment. The original packings of the α-helix, β-sheets, and statistical coils are gradually rearranged, but this cannot be observed by AFM because the lysozyme aggregations are still too small.

During the second stage (10–40 hr), more and more aromatic amino acid residues of the side chains are exposed to the border region of the protein. The α-helical secondary structures begin to transform under the influence of hydrogen bonds from nearby water, as shown by the decreasing intensity, broadened FWHM, and blue shift of the N—C_α—C stretching bands. However, no

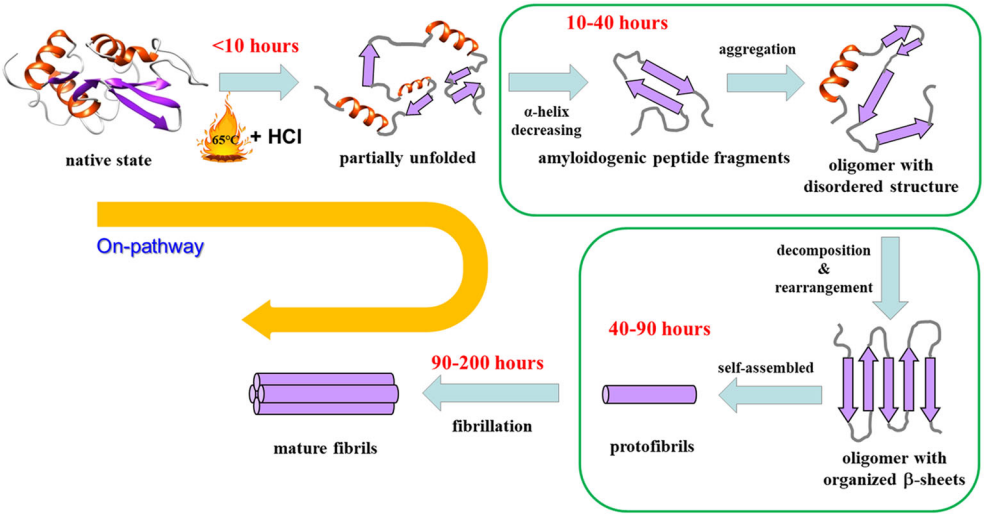

SCHEME 1 Proposed four-stage transformation mechanism of amyloid fibrillation of lysozyme under heat and acidic conditions [Colour figure can be viewed at wileyonlinelibrary.com]

organized β-sheets are immediately formed as indicated by the lack of a shift of the amide I position. Thus, the uncoiling of the α-helical structures prefers to form the statistical coils of disordered structure as the aggregation cores until reaching almost exhaustion. The oligomers formed from the core then grow larger and can now be observable in the AFM images, whereas the transmittance of the solution decreases. In addition, the oligomers with disordered structure are unstable at elevated temperature[18] and prefer to be assembled into fibrils as the amyloidogenic materials.

In the third stage (40–90 hr), almost all of the Trp and Phe residues of the side chain are exposed to the hydrophilic environment with partial unfolding of the tertiary structure. The organized β-sheet structures start to be formed between different β-strands, as indicated by the fast growth phase in the kinetic curve of the amide I position. As a result, some unbranched protofibrils are visibly formed, as seen in the AFM images, and then are gradually elongated. At the end of this stage, the population of the cross β-sheet structures is increased to saturation, but the ThT fluorescence intensity is still below half its maximum.

In the final mature stage (90–160 hr), the protofibrils are slowly assembled into mature fibrils, which are evident in AFM images. Although the Raman markers of the skeleton and side chains are almost unchanged over the incubation time, the macroscopic structural transformations of the fibrils are still ongoing. More and more cross β-sheets are formed along with the supramolecular association of the β-sheets, and thus, the ThT fluorescence intensity continues to increase. After 160 hr, the amyloid fibrils are abundant with orderly packed β-sheets and become stiff and mature.

4 | CONCLUSION

In the present study, Raman spectroscopy was applied to investigate the amyloid formation of lysozyme under a heat and acidic condition, with the aid of AFM imaging and ThT fluorescence measurements. Using the well-known Raman spectral markers for the tertiary and secondary protein structures, for example, the N—C_α—C stretching at 899 and 935 cm^{-1}, the two Trp characteristic vibrations at 760 and 1,340–1,360 cm^{-1}, the Phe residue peak at 1,003 cm^{-1}, and the amide I band near 1,650 cm^{-1}, the time-dependent denaturation kinetics of lysozyme could be directly measured.

The different kinetics of the Raman markers suggest a multistage mechanism for the amyloid formation of lysozyme. Combined with the morphology of lysozyme observed by the AFM images and the ThT fluorescence measurement, a four-stage step-by-step transformation mechanism was first proposed to describe lysozyme amyloid fibrillation under the heat and acidic conditions (pH 2.0 and 65°C): (a) unfolding of the tertiary structure to expose the aromatic amino acid residues on the side chains to the outside, (b) uncoiling of the α-helical structures to statistical coils with disordered structure, (c) decomposition of the oligomers into amyloidogenic fragment materials, and (d) formation of organized β-sheet structures with elongation of unbranched protofibrils so that cross β-sheet structures dominate, protofibrils aggregate, and the mature fibrils are finally formed.

Nevertheless, it is difficult to distinguish the disordered β-sheets from the organized (parallel and antiparallel) structures in the amide I region based only on the line shape, peak position, and intensity.[74] The amide III band has been suggested to serve as an alternative important vibrational indicator of the transformation between the cross β-sheet structure and disordered structures, because the amide III vibration is sensitive to the conformation of the peptide. A typical sharp feature around 1,230–1,240 cm^{-1} is attributed to a β-pleated sheet, whereas the disordered structure contributes a broad band near 1,240–1,245 cm^{-1}.[75] Moreover, in the deep ultraviolet Raman spectra, the contributions of various secondary structural elements such as PPII and the 2.51 helix can be characterized by the amide III_3 band: The 2.51 helix has a characteristic peak at ~1,270 cm^{-1}, whereas the amide III of PPII is substantially blue-shifted (~1,246 cm^{-1}).[76] Unfortunately, the amide III band could not be analyzed in the present spectra due to substantial interference of the hydrochloric acid solution. Thus, a new Raman marker for distinguishing disordered and organized β-sheets is needed to fully reveal the configuration transformation of the peptide skeleton during the amyloid formation of lysozyme.

ACKNOWLEDGMENTS

This work was supported by the National Natural Science Foundation of China (Grants 21573208, 21873089, and 21573210) and the National Key Basic Research Foundation of China (Grant 2013CB834602). The quantum chemical calculations were performed on the supercomputing system in the Supercomputing Center of the University of Science and Technology of China.

ORCID

Xiaoguo Zhou https://orcid.org/0000-0002-0264-0146

REFERENCES

[1] A. S. Association, *Alzheimers Dement.* **2013**, *9*, 208.

[2] F. Chiti, C. M. Dobson, *Annu. Rev. Biochem.* **2006**, *75*, 333.
[3] T. Geiger, S. Clarke, *J. Biol. Chem.* **1987**, *262*, 785.
[4] V. N. Uversky, A. L. Fink, *Biochim. Biophys. Acta* **2004**, *1698*, 131.
[5] C. M. Dobson, *Nature* **2003**, *426*, 884.
[6] J. Lee, E. K. Culyba, E. T. Powers, J. W. Kelly, *Nat. Chem. Biol.* **2011**, *7*, 602.
[7] Y. Zou, Y. Li, W. Hao, X. Hu, G. Ma, *J. Phys. Chem. B* **2013**, *117*, 4003.
[8] Y. Zou, W. Hao, H. Li, Y. Gao, Y. Sun, G. Ma, *J. Phys. Chem. B* **2014**, *118*, 9834.
[9] A. Iram, A. Naeem, *Cell Biochem. Biophys.* **2014**, *70*, 51.
[10] W. Han, K. Schulten, *J. Am. Chem. Soc.* **2014**, *136*, 35.
[11] T. D. Do, N. J. Economou, A. Chamas, S. K. Buratto, J. E. Shea, M. T. Bowers, *J. Phys. Chem. B* **2014**, *118*, 38.
[12] D. Kurouski, T. Deckert-Gaudig, V. Deckert, I. K. Lednev, *J. Am. Chem. Soc.* **2012**, *134*, 13323.
[13] K. A. Dill, J. L. MacCallum, *Science* **2012**, *338*, 1042.
[14] N. K. Holm, S. K. Jespersen, L. V. Thomassen, T. Y. Wolff, P. Sehgal, L. A. Thomsen, G. Christiansen, C. B. Andersen, A. D. Knudsen, D. E. Otzen, *Biochim. Biophys. Acta* **2007**, *1774*, 1128.
[15] B. Ma, F. Zhang, X. Wang, X. Zhu, *Int. J. Biol. Macromol.* **2017**, *98*, 717.
[16] D. R. Booth, M. Sunde, V. Bellotti, C. V. Robinson, W. L. Hutchinson, P. E. Fraser, P. N. Hawkins, C. M. Dobson, S. E. Radford, C. C. Blake, *Nature* **1997**, *385*, 787.
[17] R. Swaminathan, V. K. Ravi, S. Kumar, M. V. S. Kumar, N. Chandra, *J. Mol. Biol.* **2011**, *84*, 63.
[18] E. Frare, P. Polverino de Laureto, J. Zurdo, C. M. Dobson, A. Fontana, *J. Mol. Biol.* **2004**, *340*, 1153.
[19] J. C. Rochet, P. T. Lansbury, *Curr. Opin. Struct. Biol.* **2000**, *10*, 60.
[20] R. Mishra, K. Sörgjerd, S. Nyström, A. Nordigården, Y. C. Yu, P. Hammarström, *J. Mol. Biol.* **2007**, *366*, 1029.
[21] R. A. Karaballi, S. Merchant, S. R. Power, C. L. Brosseau, *Phys. Chem. Chem. Phys.* **2018**, *20*, 4513.
[22] M. Tabatabaei, F. A. Caetano, F. Pashee, S. S. Ferguson, F. Lagugné-Labarthet, *Analyst* **2017**, *142*, 4415.
[23] T. Deckert-Gaudig, V. Deckert, *Sci. Rep.* **2016**, *6*, 39622.
[24] D. Kurouski, R. P. Van Duyne, I. K. Lednev, *Analyst* **2015**, *140*, 4967.
[25] V. Sereda, I. K. Lednev, *J. Raman Spectrosc.* **2014**, *45*, 665.
[26] S. Jain, J. B. Udgaonkar, *J. Mol. Biol.* **2008**, *382*, 1228.
[27] S. E. Hill, J. Robinson, G. Matthews, M. Muschol, *Biophys. J.* **2009**, *96*, 3781.
[28] M. Yang, C. Dutta, A. Tiwari, *J. Phys. Chem. B* **2015**, *119*, 3969.
[29] V. K. Ravi, M. Goel, H. C. Kotamarthi, S. R. K. Ainavarapu, R. Swaminathan, *PLoS One* **2014**, *9*, e87012.
[30] Y. Li, J. Maurer, A. Roth, V. Vogel, E. Winter, W. Mäntele, *Rev. Sci. Instrum.* **2014**, *85*, 084302.
[31] V. Shashilov, M. Xu, N. Makarava, R. Savtchenko, I. V. Baskakov, I. K. Lednev, *J. Phys. Chem. B* **2012**, *116*, 7926.
[32] D. Kurouski, T. Deckert-Gaudig, V. Deckert, I. K. Lednev, *Biophys. J.* **2014**, *106*, 263.
[33] S. Bonhommeau, D. Talaga, J. Hunel, C. Cullin, S. Lecomte, *Angew. Chem.* **2017**, *129*, 1797.
[34] D. Kurouski, T. Postiglione, T. Deckert-Gaudig, V. Deckert, I. K. Lednev, *Analyst* **2013**, *138*, 1665.
[35] L. A. Popova, R. Kodali, R. Wetzel, I. K. Lednev, *J. Am. Chem. Soc.* **2010**, *132*, 6324.
[36] V. Shashilov, M. Xu, V. V. Ermolenkov, L. Fredriksen, I. K. Lednev, *J. Am. Chem. Soc.* **2007**, *129*, 6972.
[37] C. Ortiz, D. Zhang, A. E. Ribbe, Y. Xie, D. Ben-Amotz, *Biol. Chem.* **2007**, *128*, 150.
[38] M. M. Apetri, N. C. Maiti, M. G. Zagorski, P. R. Carey, V. E. Anderson, *J. Mol. Biol.* **2006**, *355*, 63.
[39] M. Sorci, R. A. Grassucci, I. Hahn, J. Frank, G. Belfort, *Proteins* **2009**, *77*, 62.
[40] M. Xu, V. V. Ermolenkov, V. N. Uversky, I. K. Lednev, *J. Biophotonics* **2008**, *1*, 215.
[41] M. Xu, V. V. Ermolenkov, W. He, V. N. Uversky, L. Fredriksen, I. K. Lednev, *Biopolymers* **2005**, *79*, 58.
[42] I. W. Hamley, *Angew. Chem. Int. Ed.* **2007**, *46*, 8128.
[43] V. A. Shashilov, V. Sikirzhytski, L. A. Popova, I. K. Lednev, *Methods* **2010**, *52*, 23.
[44] M. Xu, V. Shashilov, I. K. Lednev, *J. Am. Chem. Soc.* **2007**, *129*, 11002.
[45] V. A. Shashilov, I. K. Lednev, *J. Am. Chem. Soc.* **2008**, *130*, 309.
[46] M. R. Krebs, E. H. Bromley, A. M. Donald, *J. Struct. Biol.* **2005**, *149*, 30.
[47] R. Khurana, C. Coleman, C. Ionescu-Zanetti, S. A. Carter, V. Krishna, R. K. Grover, R. Roy, S. Singh, *J. Struct. Biol.* **2005**, *151*, 229.
[48] M. Biancalana, S. Koide, *Biochim. Biophys. Acta* **2010**, *1804*, 1405.
[49] S. Y. Ow, D. E. Dunstan, *Soft Matter* **2013**, *9*, 9692.
[50] L. Chen, W. Zhu, K. Lin, N. Hu, Y. Yu, X. Zhou, L. F. Yuan, S. M. Hu, Y. Luo, *J. Phys. Chem. A* **2015**, *119*, 3209.
[51] K. Lin, X. G. Zhou, Y. Luo, S. L. Liu, *J. Phys. Chem. B* **2010**, *114*, 3567.
[52] K. Lin, X. G. Zhou, S. L. Liu, Y. Luo, *Chin. J. Chem. Phys.* **2013**, *26*, 121.
[53] K. Lin, N. Hu, X. G. Zhou, S. L. Liu, Y. Luo, *J. Raman Spectrosc.* **2012**, *43*, 82.
[54] C. Q. Tang, K. Lin, X. G. Zhou, S. L. Liu, *Chin. J. Chem. Phys.* **2016**, *29*, 129.
[55] M. Chen, R. Lord, R. Mendelsohn, *J. Am. Chem. Soc.* **1974**, *96*, 3038.
[56] J. A. Sweeney, S. A. Asher, *J. Phys. Chem.* **1990**, *94*, 4784.
[57] V. Kocherbitov, J. Latynis, A. Misiūnas, J. Barauskas, G. Niaura, *J. Phys. Chem. B* **2013**, *117*, 4981.
[58] Z. Q. Wen, *J. Pharm. Sci.* **2007**, *96*, 2861.
[59] T. G. Spiro, B. P. Gaber, *Annu. Rev. Biochem.* **1977**, *46*, 553.
[60] R. Lord, N. T. Yu, *J. Mol. Biol.* **1970**, *50*, 509.
[61] M. Tsuboi, M. Suzuki, S. A. Overman, G. J. Thomas, *Biochemistry* **2000**, *39*, 2677.
[62] D. I. Ellis, D. P. Cowcher, L. Ashton, S. O'Hagan, R. Goodacre, *Analyst* **2013**, *138*, 3871.

[63] S. Mangialardo, L. Gontrani, F. Leonelli, R. Caminiti, P. Postorino, *RSC Adv.* **2012**, *2*, 12329.

[64] R. Schweitzer-Stenner, *J. Phys. Chem. B* **2012**, *116*, 4141.

[65] T. J. Measey, R. Schweitzer-Stenner, *J. Am. Chem. Soc.* **2006**, *128*, 13324.

[66] I. Harada, T. Miura, H. Takeuchi, *Spectrochim. Acta A* **1986**, *42*, 307.

[67] M. N. Siamwiza, R. C. Lord, M. C. Chen, T. Takamatsu, I. Harada, H. Matsuura, T. Shimanouchi, *Biochemistry* **1975**, *14*, 4870.

[68] F. Chiti, C. M. Dobson, *Annu. Rev. Biochem.* **2017**, *86*, 27.

[69] L. Xing, K. Lin, X. Zhou, S. Liu, Y. Luo, *J. Phys. Chem. B* **2016**, *120*, 10660.

[70] M. Chen, R. Lord, R. Mendelsohn, *Biochim. Biophys. Acta* **1973**, *328*, 252.

[71] I. V. Stokkum, H. Linsdell, J. Hadden, P. Haris, D. Chapman, M. Bloemendal, *Biochemistry* **1995**, *34*, 10508.

[72] A. Hédoux, J. Willart, R. Ionov, F. Affouard, Y. Guinet, L. Paccou, A. Lerbret, M. Descamps, *J. Phys. Chem. B* **2006**, *110*, 22886.

[73] A. Hédoux, R. Ionov, J. F. Willart, A. Lerbret, F. Affouard, Y. Guinet, M. Descamps, D. Prevost, L. Paccou, F. Danede, *J. Chem. Phys.* **2006**, *124*, 014703.

[74] J. T. Pelton, L. R. McLean, *Anal. Biochem.* **2000**, *277*, 167.

[75] A. Rygula, K. Majzner, K. Marzec, A. Kaczor, M. Pilarczyk, M. Baranska, *J. Raman Spectrosc.* **2013**, *44*, 1061.

[76] I. K. Lednev, V. V. Ermolenkov, S. Higashiya, L. A. Popova, N. I. Topilina, J. T. Welch, *Biophys. J.* **2006**, *91*, 3805.

SUPPORTING INFORMATION

Additional supporting information may be found online in the Supporting Information section at the end of the article.

How to cite this article: Xing L, Fan W, Chen N, Li M, Zhou X, Liu S. Amyloid formation kinetics of hen egg white lysozyme under heat and acidic conditions revealed by Raman spectroscopy. *J Raman Spectrosc*. 2019;50:629–640. https://doi.org/10.1002/jrs.5567